Corrosion products on biomedical magnesium alloy soaked in simulated body fluids

Yunchang Xin
Advanced Materials Institute, Tsinghua University, Shenzhen Graduate School, Shenzhen 518055, China; and Department of Physics and Materials Science, City University of Hong Kong, Kowloon, Hong Kong, China

Kaifu Huo
Department of Physics and Materials Science, City University of Hong Kong, Kowloon, Hong Kong, China; and Hubei Province Key Laboratory of Refractories and Ceramics, College of Materials and Metallurgy, Wuhan University of Science and Technology, Wuhan 430081, China

Tao Hu
Department of Physics and Materials Science, City University of Hong Kong, Kowloon, Hong Kong, China

Guoyi Tang[a)]
Advanced Materials Institute, Tsinghua University, Shenzhen Graduate School, Shenzhen 518055, China

Paul K. Chu[b)]
Department of Physics and Materials Science, City University of Hong Kong, Kowloon, Hong Kong, China

(Received 3 November 2008; accepted 4 February 2009)

Magnesium alloys are potential materials in biodegradable hard tissue implants. Their degradation products in the physiological environment not only affect the degradation process but also influence the biological response of bone tissues. In the work reported here, the composition and structure of the corrosion product layer on AZ91 magnesium alloy soaked in a simulated physiological environment, namely simulated body fluids (SBFs), are systematically investigated using secondary electron microscopy (SEM), Fourier transform infrared (FTIR) spectroscopy, x-ray photoelectron spectroscopy (XPS), x-ray diffraction (XRD), and in situ monitoring of the corrosion morphology. Our results show that the corrosion product layer comprises mainly amorphous magnesium (calcium) phosphates, magnesium (calcium) carbonates, magnesium oxide/hydroxide, and aluminum oxide/hydroxide. The magnesium phosphates preferentially precipitate at obvious corrosion sites and are present uniformly in the corrosion product layer, whereas calcium phosphates nucleate at passive sites first and tend to accumulate at isolated and localized sites. According to the cross sectional views, the corrosion product layer possesses a uniform structure with thick regions several tens of micrometers as well as thin areas of several micrometers in some areas. Localized corrosion is the main reason for the nonuniform structure as indicated by the pan and cross-sectional views. The results provide valuable information on the cytotoxicity of magnesium alloys and a better understanding on the degradation mechanism of magnesium alloys in a physiological environment.

I. INTRODUCTION

Because of their unique mechanical properties and biodegradability, Mg-based alloys are potential biodegradable hard tissue implants. Good biocompatibility has been observed in earlier clinical studies and in many in vivo and in vitro experiments.[1–3] Some studies have also shown that dissolved magnesium ions may promote bone tissue growth.[4–7] However, attacks by aggressive ions in body fluids such as chlorides, hydrocarbonates, and sulfates lead to fast surface corrosion on Mg-based biomedical implants.[8–11] Many in vivo experiments have been carried out to study the degradation process and corresponding tissue responses such as cytotoxicity and side effects from Mg degradation.[3,7,12,13] Serious corrosion has been observed to take place after implantation and a surface layer composed of Mg, Ca, and P forms on the implants. However, the fast degradation does not lead to a higher serum level of magnesium.[7] The nature of this corrosion product layer not only influences the

Address all correspondence to these authors.
[a)]e-mail: tanggy@mail.sz.tsinghua.edu.cn
[b)]e-mail: paul.chu@cityu.edu.hk
DOI: 10.1557/JMR.2009.0323

subsequent degradation process,[8] but also might affect the biological response of bone tissues to the implants. This corrosion products layer generally composed of magnesium and calcium phosphates, as well as magnesium oxides,[14–16] but the precipitation process, detailed structure, and corrosion product evolution have not been fully disclosed. It is well known that various alloying elements are incorporated into Mg to improve the mechanical properties and/or corrosion resistance. The alloying elements influence the structure of the materials and impact the corrosion performance including the surface morphology, corrosion resistance, and corrosion products. In biomedical applications, the cytoxicity of these alloying elements needs to be clarified. In fact, the influence of these alloying elements on the cytotoxicity is mainly in the form of corrosion products including dissolved ions and precipitated corrosion products on the implant surface. Different types of magnesium alloys such as Al-Zn–containing alloy (such as AZ91, AZ31), rare earth containing alloys (such as WE-43, LAE442), and Ca-containing Mg alloys[3,13] have been proposed as candidates in biodegradable implants. Before clinical applications, it is necessary to obtain more detailed information about the corrosion products on these magnesium alloys. A better understanding of the corrosion products helps to evaluate the safety of these implants and elucidate the corrosion process and mechanism in a physiological environment. In our previous work,[17] the corrosion behavior of the AZ91 magnesium alloy was systematically studied. However, detailed information about the structure and composition of the corrosion product layer and their evolution with immersion duration are not well known.

In the work reported here, immersion tests were conducted in a simulated physiological environment by immersion in simulated body fluids (SBFs). The structure of the corrosion product layer, phase constituents, and their distributions were studied by scanning electron microscopy (SEM), energy-dispersive x-ray analysis (EDS), Fourier transform infrared (FTIR) spectroscopy, x-ray photoelectron spectroscopy (XPS), and x-ray diffraction (XRD). The mechanisms responsible for the different distributions and the tendency of the constituents were studied. In addition, the evolution of the corrosion products with immersion time was evaluated. This study aims at providing important information on the cytotoxicity and a better understanding of the degradation mechanism of magnesium alloys in a physiological environment.

II. EXPERIMENTAL DETAILS

A. Sample preparation

The commercially available die cast AZ91 magnesium alloy was used in our experiments. The composition of the alloy is shown in Table I. The as-received materials were cut into 15 × 15 × 3-mm blocks. The samples were ground, polished, and ultrasonically cleaned in alcohol. The samples were put into a bottle containing 50 mL SBF for 2 min, 30 min, 1 day, 3 days, or 5 days at 37 ± 0.5 °C. The ion concentrations in the SBF are similar to those in human plasma[18] and shown in Table II. After immersion, the samples were taken out of the solutions, cleaned using distilled water, and dried.

B. Optical microscopy and SEM observation

The as-polished samples were immersed in a dish with SBF. In situ observation of the corrosion morphology was performed directly by optical microscopy. The top surface and cross-sectional structure of the corrosion product layer after exposure in SBF were observed by SEM (S-4700; Hitachi, Tokyo, Japan). Before the cross-sectional observation, the soaked samples were attached to the metal holder using paint and ground, polished, and carbon coated. The composition of the corrosion products in selective regions were determined by EDS.

C. Characterization

XRD (Cu K_α radiation, 40 kV, 30 mA) was used to determine the phase constituents in the corrosion product layer. However, in direct measurement of the soaked samples, no information was gained from the corrosion product layer except peaks originating from the substrate Mg and $Mg_{17}Al_{12}$ phase (β phase). Thus, we scraped off the corrosion products using a stainless steel knife, and XRD was performed on the powders to acquire more detailed information. Before scraping, the knife was ultrasonically cleaned in alcohol to get rid of contamination. The functional groups in the corrosion product

TABLE I. Elemental composition of AZ91 magnesium alloy.

	Al (wt%)	Zn (wt%)	Mn (wt%)	Si (wt%)	Fe (wt%)	Ni (wt%)	Cu (wt%)
AZ91	8.5–9.5	0.45–0.9	0.17–0.5	<0.05	<0.004	<0.001	<0.015

TABLE II. Ion concentrations in SBFs.

Concentration (mmol/L)	Na^+	K^+	Ca^{2+}	Mg^{2+}	HCO_3^-	Cl^-	HPO_4^{2-}	SO_4^{2-}
SBF	142.0	5.0	2.5	1.5	4.2	148.5	1.0	0.5

layer were determined by FTIR from 4000 to 400 cm^{-1}. The elemental binding energies were determined by XPS (PH5802; Physical Electronics, Chanhassen, MN) with Al K_α excitation. The power was 350 W and take-off angle was 45°.

III. RESULTS AND DISCUSSION

A. Structure of the corrosion layer

To get rid of the damage on the surface corrosion product layer by ultrasonic cleaning and the influence from the residual test solution, the sample was rinsed by shaking the soaked sample in distilled water numerous times with the aid of a pair of tweezers. The SEM micrographs and corresponding EDS results acquired from selected regions on the sample soaked in SBF for 1 day are depicted in Fig. 1. Serious corrosion can be observed on the entire sample surface. Isolated white regions with many cracks are embedded in the gray surface. Mg, Al, Zn, O, and P can be detected from the gray area, implying that this region contains magnesium phosphates and $MgO/Mg(OH)_2$. It is more difficult to identify whether Al arises from the $Al_2O_3/Al(OH)_3$, β phase ($Mg_{17}Al_{12}$), or Al dissolved in the substrate. The white regions contain a large amount of Ca in addition to Mg, Al, Zn, O, and P, and both the P and O weight percents increase significantly. The atomic ratio of Ca to P is ~0.32, which is much lower than that in calcium phosphate (3:2). Thus, it can be inferred that these regions contain both calcium phosphates and magnesium phosphates. Figure 2 shows the SEM micrographs and EDS results acquired from the samples after immersion in SBF for 3 days. The area of the white region increases, and the Ca and P contents increase significantly. The EDS data acquired from the gray region are similar to those obtained after 1-day immersion. As shown in Fig. 3, the morphology after immersion in SBF for 5 days is similar to that of the sample after immersion for 3 days. The elemental compositions obtained from both the gray and white regions are similar to that of the sample after immersion for 3 days. These results show that the corrosion product layer contains magnesium phosphate, calcium phosphates, and magnesium oxide or hydroxide. Magnesium phosphates are present uniformly, whereas calcium phosphates appear preferentially in many isolated regions. The calcium phosphate content increases with immersion time and becomes stable after 3 days of exposure. The presence of cracks probably results from surface shrinkage because of dehydration of the corrosion products after drying in warm air and inside the SEM vacuum chamber.

The different distributions of magnesium phosphates and calcium phosphates probably stem from the corrosion behavior in SBF. Two sets of experiments are designed to unravel the difference. The pictures taken from the sample immersed in SBF after 2, 5, and 30 min are shown in Fig. 4. On exposure to the solution, corrosion takes place on many sites, leading to hydrogen bubble formation. As time elapses, the corroded sites

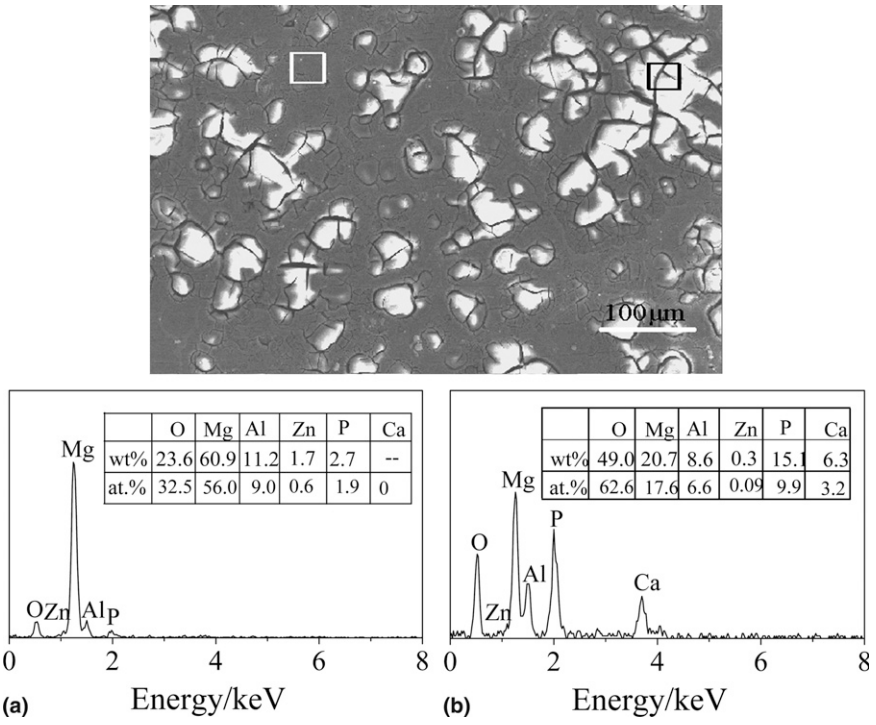

FIG. 1. SEM micrograph of AZ91 magnesium alloy soaked in SBF for 1 day and EDS results at selective regions: (a) EDS results in the white square region and (b) EDS results in the black square region.

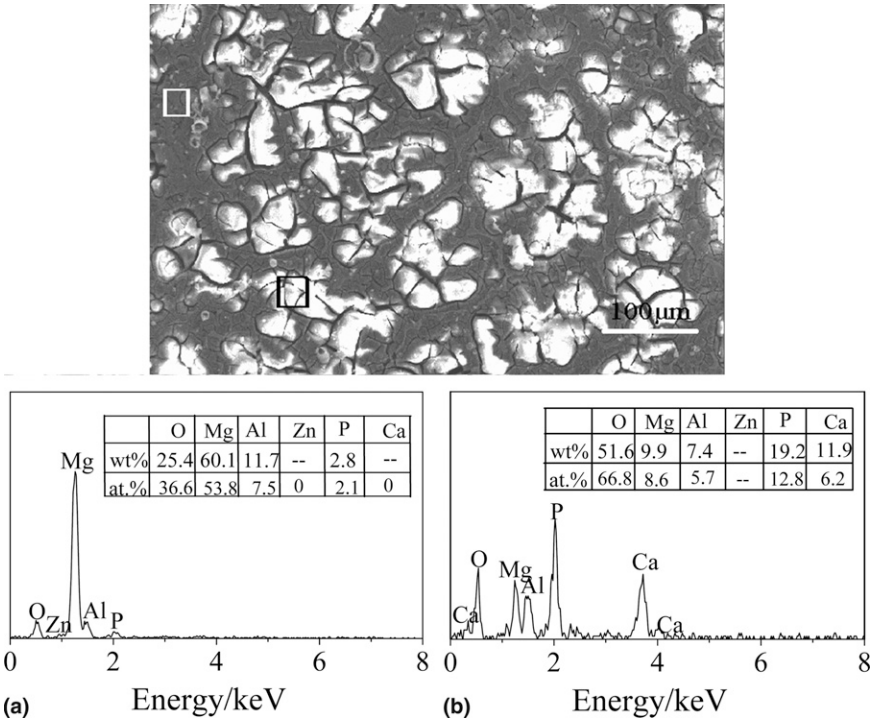

FIG. 2. SEM micrograph of AZ91 magnesium alloy soaked in SBF for 3 days and EDS results at selective regions: (a) EDS results in the white square region and (b) EDS results in the black square region.

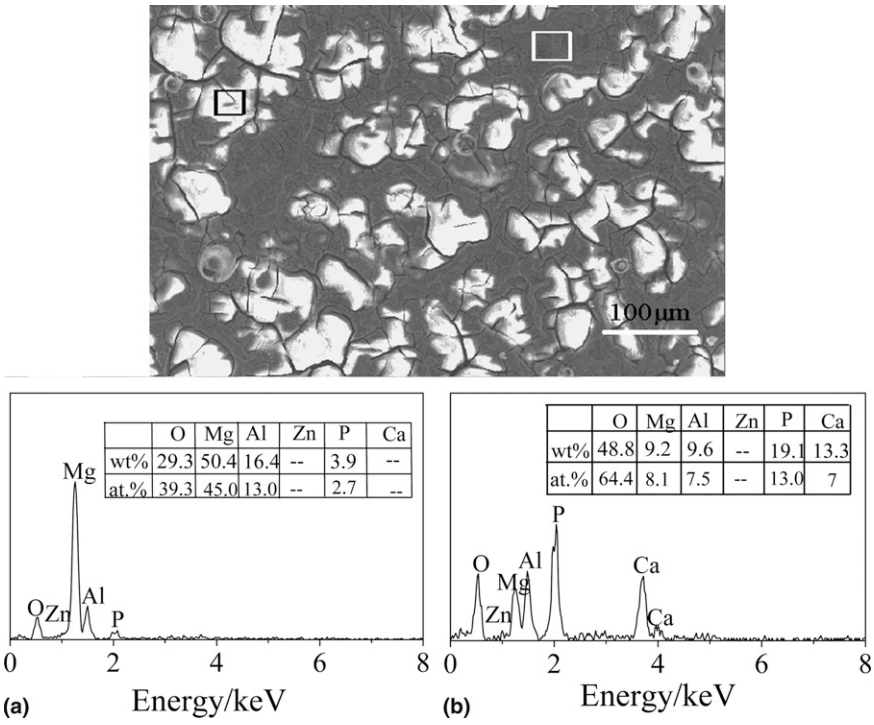

FIG. 3. SEM micrograph of AZ91 magnesium alloy soaked in SBF for 5 days and EDS results at selective regions: (a) EDS results in the white square region and (b) EDS results in the black square region.

expand laterally. However, these corrosion sites (black areas) tend to be passive because of precipitation of the corrosion products.[9] Meanwhile, corrosion occurs rapidly at other vulnerable sites as indicated by hydrogen evolution. The morphology and composition of the precipitates at these corrosion sites are studied by SEM and EDS, and the results are shown in Fig. 5. Many white bumps (denoted by a white arrow) corresponding to

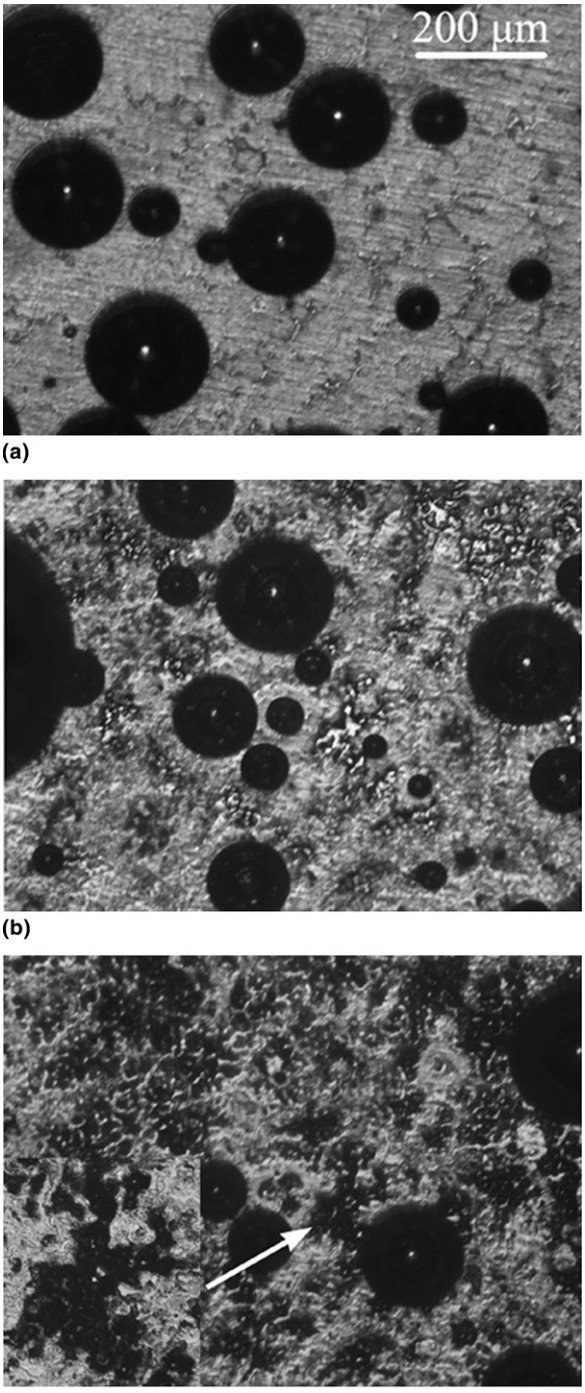

FIG. 4. In situ observation of the AZ91 magnesium alloy immersed in SBF by optical microscopy: (a) morphology after immersion for 2 min, (b) morphology after immersion for 10 min, and (c) morphology after immersion for 30 min. The inside picture in (c) is the higher magnification view of the region denoted by the white arrow.

the sites of hydrogen evolution are observed. The EDS spectra obtained from these sites show that this region is mainly composed of Mg, Al, O, and P, but no obvious Ca peaks are observed. The results imply that magnesium phosphates are preferentially precipitated compared with calcium phosphates. In the plain region, only peaks from Mg and Al can be seen, but not O and P, suggesting that almost no corrosion takes place at these regions. These data confirm selective punch-through during corrosion of the surface. Magnesium dissolution results in significant enhancement in the local pH value at the corrosion sites[13,19] because of the formation of magnesium hydroxide and magnesium phosphates. The local concentration of magnesium ions at the corrosion sites should be high, and hence, magnesium phosphates are much easier to precipitate than calcium phosphates. In an aqueous solution, surface-absorbed magnesium ions can inhibit nucleation of calcium phosphates.[20] The high local concentration of magnesium ions also impedes precipitation of calcium phosphates. Therefore, magnesium phosphates are preferentially precipitated compared with calcium phosphates. After the whole surface has undergone corrosion, magnesium phosphates will cover the entire surface. As shown in Fig. 5(b), after a 30-min immersion in SBF, many white regions with cracks emerge (denoted by a white arrow). These regions contain mainly Mg, Al, O, P, and Ca, indicating the presence of calcium phosphates. These regions should correspond to the passive regions (black area) observed by optical microscopy. In the region denoted by a white square, besides peaks arising from Mg, only a weak peak from O is observed. Oxygen may come from magnesium hydroxide. At these regions, little corrosion occurs. The original pH of the solution is ~7.42. After a longer exposure time, the pH value of the whole solution increases dramatically to nearly 10 because of by-products resulting from magnesium dissolution, OH^-,[13] and calcium phosphates preferentially nucleating at passive regions, as corroborated by the SEM and EDS results. It is difficult for calcium phosphates to precipitate at the corrosion sites because of the high local concentration of magnesium ions and the high evolution rate of hydrogen. Nonetheless, when the nuclei form at passive sites, calcium phosphates grow more easily at these passive regions than at regions without nucleation. Finally, nonuniform distributions of calcium phosphates in the corrosion product layer result.

The cross-sectional views of the samples soaked in SBF for 1, 3, and 5 days together with the EDS results obtained from selected regions are exhibited in Fig. 6. The morphologies after different exposure periods are similar, but the corrosion products layer is not uniform. The layer is thin in most regions but can be very thick at some other locations. The sites with thick corrosion products can be ascribed to corrosion penetrating into the substrate and gradual precipitation of the corrosion products. This cross-section indicates a nonuniform corrosion process on the sample surface. Severe corrosion occurs preferentially at many isolated sites and subsequently penetrates into the materials significantly. Such local corrosion is common during corrosion of

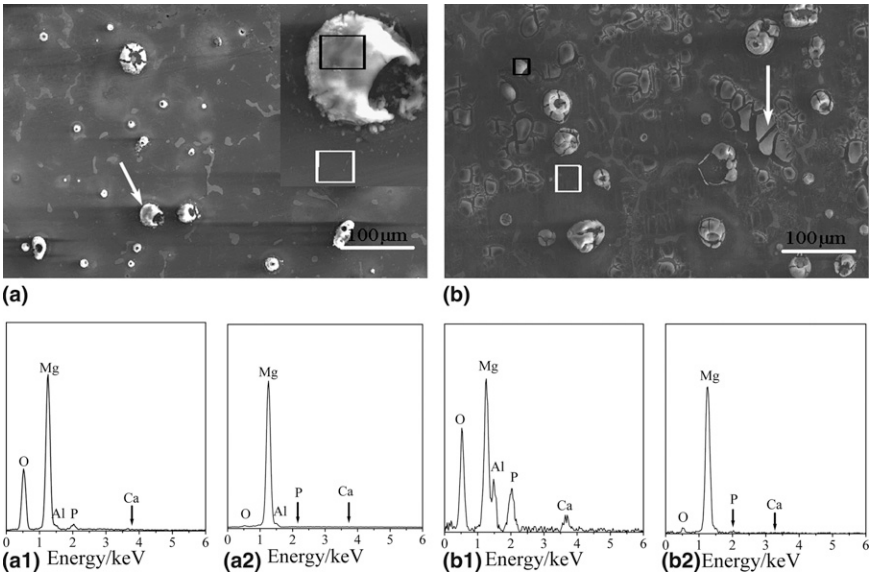

FIG. 5. SEM micrographs of AZ91 magnesium alloy soaked in SBF for 2 and 30 min and EDS results at selective regions: (a) SEM micrograph after 2-min immersion, (a_1) EDS results in the black square region in (a), (a_2) EDS results in the white square region in (a), (b) SEM micrograph after 30-min immersion, (b_1) EDS results in the black square region in (b), and (b_2) EDS results in the white square region in (b).

magnesium alloys and mainly results from the presence of partially protective films.[20] However, in accordance with the cross-sectional views, this local corrosion does not induce pitting corrosion caused by precipitation of the corrosion products. The EDS results show that the thick corrosion product layer region contains a large amount of Ca and P in addition to Mg, O, and Al. As the immersion time increases, both the Ca and P contents increase, but from days 3 to 5, the changes are not as obvious. SEM can provide high-magnification views of the corrosion products allowing analysis of the composition of the corrosion products. However, dehydration of the corrosion products layer produces many cracks on the corrosion product layer, thereby possibly altering the original morphology.

B. Composition of corrosion products

The XRD spectra acquired from the corrosion products are shown in Fig. 7. Two broad bands centered at ~31 and 42° denoted by arrows are observed. However, the strongest peaks of magnesium and calcium phosphate are near 30°. It is thus difficult to discern the exact constituents. Here, the XRD results only indicate that all the corrosion products are amorphous.

The FTIR spectra acquired from samples soaked in SBF for 1, 3, and 5 days are depicted in Fig. 8. The broad absorption band from 3700 to 2500 cm^{-1} is attributed to the stretching vibration of the OH^- group.[21] The band at 1640 cm^{-1} arises from H_2O bending vibration.[22] Absorption bands at 1435, 1488, and 850 cm^{-1} correspond to carbonates.[22] The band at ~578 cm^{-1} is induced by magnesium hydroxides. The 450-cm^{-1} band can be ascribed to Mg–O bonding (MgO).[23] The three spectra are similar, and the corrosion products are probably similar also. Based on the FTIR result, the corrosion product layer contains $MgO/Mg(OH)_2$, phosphates, and carbonates. According to Canham et al.,[24] a sharp P−O bending mode doublet at 600 cm^{-1} is indicative of hydroxyapatite. No such absorption mode is observed from the three spectra. Hence, it can be inferred that the corrosion products contain common calcium phosphates and not hydroxyapatite.

To obtain more detailed information on the constituents in the corrosion product layer, XPS is used to examine the elemental chemical states. The full spectra and high-resolution spectra of P, C, and Al are depicted in Fig. 9. The three full spectra are similar, and Mg, Al, P, C, and O peaks are present. The high-resolution spectra of P 2p exhibit two peaks. The two peaks centered at 133.2 and 133.9 eV originate from bonding between PO_4^{3-} and Mg in the form of magnesium phosphates and bonding between PO_4^{3-} and Ca in the form of calcium phosphates, respectively.[25,26] The contents of calcium phosphates in the total phosphates in the corrosion product layer after immersion for 3 days (72.0%) and immersion for 5 days (63.3%) are both much higher than that after immersion for 1 day (44.9%). The results are consistent with the EDS data. The high-resolution spectra of C1s can be deconvoluted into three peaks at ~284.6, 286.1, and 288.5 eV. The bands at 284.6 and 286.1 eV correspond to bonds from C–C (and/or C–H) and C–O, respectively,[27] and both of them result from surface contamination. The band at 288.5 eV is indicative

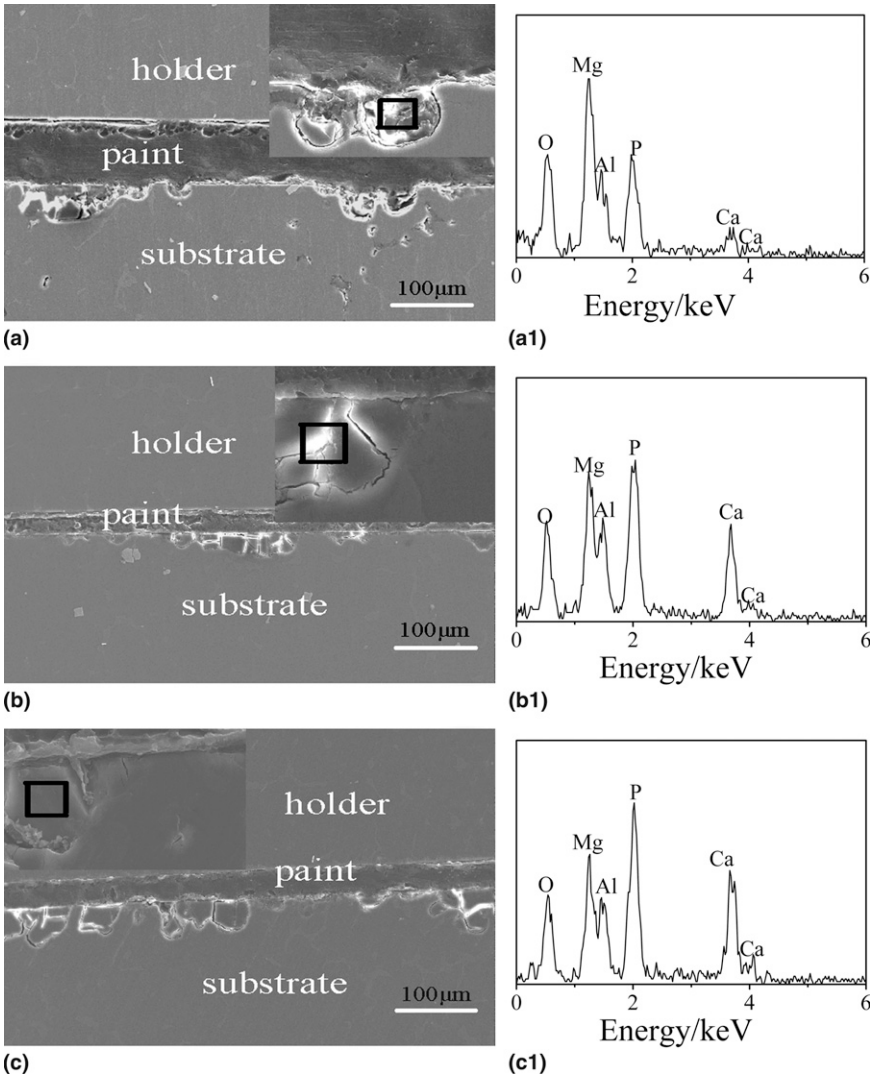

FIG. 6. Cross-section SEM micrographs of the corrosion product layer and EDS results at selective regions: (a) SEM micrograph of sample after 1-day immersion, (a_1) EDS results at selection region in (a), (b) SEM micrograph of sample after 3-day immersion, (b_1) EDS results at selection region in (b), (c) SEM micrograph of sample after 5-day immersion, and (c_1) EDS results at selection region in (c).

of carbonates,[28] confirming the presence of magnesium and/or calcium carbonates in the corrosion products. The high-resolution spectra of Al 2p are also acquired. The two peaks located at 74.3 and 75.4 eV originate from Al in the form of Al_2O_3 and $Al(OH)_3$, respectively.[29] With prolonged exposure time, the ratio of $Al(OH)_3$: Al_2O_3 increases.

It can be concluded that the corrosion products after immersion for 1, 3, and 5 days are similar and they consist of MgO, $Mg(OH)_2$, Al_2O_3, $Al(OH)_3$, magnesium, and calcium phosphates, as well as magnesium and calcium carbonates, but the relative contents vary with different exposure duration. These corrosion products are all amorphous. The formation mechanism of these corrosion products can be deduced from the corrosion process. On exposure to an aqueous solution, the following reaction takes place[20]:

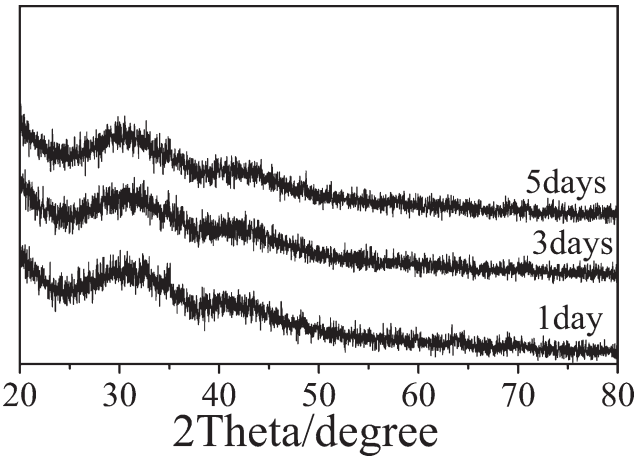

FIG. 7. XRD spectra obtained from the corrosion products of the AZ91 magnesium alloy after soaking in SBF for 1, 3, and 5 days.

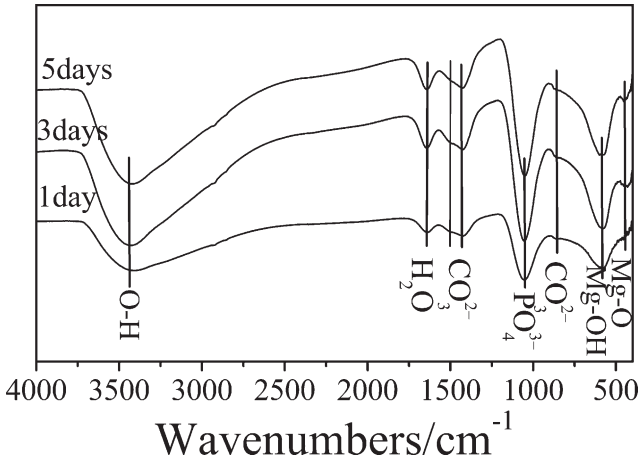

FIG. 8. FTIR spectra acquired from the AZ91 magnesium alloy soaked in SBF for 1, 3, and 5 days.

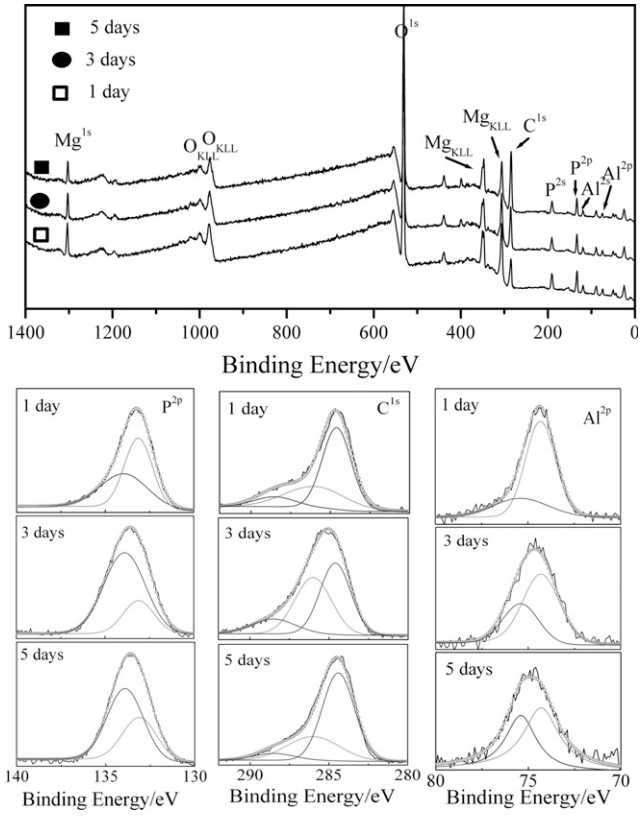

FIG. 9. XPS spectra acquired from the AZ91 magnesium alloy after soaking in SBF for 1, 3, and 5 days.

$$Mg + 2\,H_2O \rightarrow Mg^{2+} + 2OH^- + H_2 \quad . \qquad (1)$$

Magnesium dissolution generates a large amount of OH^-. Increase in the pH value leads to MgO or $Mg(OH)_2$ precipitates. The β ($Mg_{17}Al_{12}$) phase has a higher standard potential than either Mg or Al and exhibits a passive behavior over a wide pH range. Therefore, corrosion of the β phase should be limited. In fact, they often fall off from the surface because of selective attack along the boundary of the Mg substrate and β phase.[20] In the AZ91 magnesium alloy, besides the Al in β phase, a large amount of Al dissolves in the Mg substrate.[20] The Al_2O_3, and $Al(OH)_3$ mainly come from corrosion of the dissolved aluminum in the substrate. Insoluble magnesium and calcium phosphates and carbonates can also precipitate in the corrosion products according to the following reactions:

$$3\,Mg^{2+}(\text{or } Ca^{2+}) + 2\,OH^- + 2\,HPO_4^{2-} + (n-2)H_2O \rightarrow Mg_3(\text{or Ca})(PO_4)_2 \cdot nH_2O \quad , \qquad (2)$$

$$Mg^{2+}(\text{or } Ca^{2+}) + OH^- + HCO_3^{2-} + (n-1)H_2O \rightarrow Mg(\text{or Ca})CO_3 \cdot nH_2O \quad . \qquad (3)$$

From the biological point of view, magnesium phosphates and carbonates, as well as calcium phosphates and carbonates, possess favorable biocompatibility.[30–32] Al_2O_3 is also biocompatible,[33] but the biological responses of $Al(OH)_3$, MgO, and $Mg(OH)_2$ are not yet clear.

IV. CONCLUSION

A systematic study was performed to determine the structure, constituents, and phase distribution of the corrosion products on AZ91 magnesium alloy on exposure to SBFs for different periods of time. The pertinent mechanisms were discussed. Our results showed that the corrosion product layer is mainly composed of amorphous magnesium (calcium) phosphates, magnesium (calcium) carbonates, magnesium oxide/hydroxide, and aluminum oxide/hydroxide. Magnesium phosphates are present in the product layer uniformly, whereas calcium phosphates nucleate preferentially at passive local sites and evolve gradually. Because of local corrosion at vulnerable sites, the corrosion product layer is not uniform as verified by the cross-sectional and surface views. Corrosion is observed to penetrate into the substrate, and nonuniform precipitation of the corrosion products leads to thick corrosion product layer at some sites but thin ones in other regions.

ACKNOWLEDGMENTS

This project was supported by City University of Hong Kong Applied Research Grant (ARG) 9667002, Key Grant Project of Educational Commission of Hubei Province Z200711001, and Chenguang Project for Youth of Wuhan City.

REFERENCES

1. E.D. McBride: Absorbable metal in bone surgery. *J. Am. Med. Assoc.* **111,** 2464 (1938).
2. J. Vormann: Magnesium: Nutrition and metabolism. *Mol. Aspects Med.* **24,** 27 (2003).
3. F. Witte, V. Kaese, H. Haferkamp, E. Switzer, A. Meyer-Lindenberg, C.J. Wirth, and H. Windhagen: In vivo corrosion of four magnesium

alloys and the associated bone response. *Biomaterials* **26,** 3557 (2005).
4. H. Zreiqat, C.R. Howlett, A. Zannettino, P. Evans, G. Schulze-Tanzil, C. Knabe, and M. Shakibaei: Mechanisms of magnesium-stimulated adhesion of osteoblastic cells to commonly used orthopaedic implants. *J. Biomed. Mater. Res.* **62,** 175 (2002).
5. P.A. Revell, E. Damien, X.S. Zhang, P. Evans, and C.R. Howlett: The effect of magnesium ions on bone bonding to hydroxyapatite. *Key Eng. Mater.* **254,** 447 (2004).
6. Y. Yamasaki, Y. Yoshida, M. Okazaki, A. Shimazu, T. Kubo, Y. Akagawa, and T. Uchida: Action of FG-$MgCO_3$ Ap-collagen composite in promoting bone formation. *Biomaterials* **24,** 4913 (2003).
7. M.P. Staiger, A.M. Pietak, J. Huadmai, and G. Dias: Magnesium and its alloys as orthopedic biomaterials: A review. *Biomaterials* **27,** 1728 (2006).
8. Y.C. Xin, K.F. Huo, T. Hu, G.Y. Tang, and P.K. Chu: Influence of aggressive ions on the degradation behavior of biomedical magnesium alloy in physiological environment. *Acta Biomater.* **4,** 2008 (2008).
9. G.L. Song and A. Atrens: Understanding magnesium corrosion—A framework for improved alloy performance. *Adv. Eng. Mater.* **5,** 837 (2003).
10. N.C. Quach, P.J. Uggowitzer, and P. Schmutz: Corrosion behaviour of an Mg-Y-RE alloy used in biomedical applications studied by electrochemical techniques. *C.R. Chim.* **11,** 1043 (2008).
11. H. Kuwahara, Y. Al-Abdullat, M. Ohta, S. Tsutsumi, K. Ikeuchi, and N. Mazaki: Surface reaction of magnesium in Hank's solutions. *Mater. Sci. Forum* **350,** 349 (2000).
12. L.P. Xu, G.N. Yu, E. Zhang, F. Pan, and K. Yang: In vivo corrosion behavior of Mg-Mn-Zn alloy for bone implant application. *J. Biomed. Mater. Res.* **83,** 703 (2007).
13. Z.J. Li, X.N. Gu, S.Q. Lou, and Y.F. Zheng: The development of binary Mg-Ca alloys for use as biodegradable materials within bone. *Biomaterials* **29,** 1329 (2008).
14. L.C. Li, J.C. Gao, and Y. Wang: Evaluation of cyto-toxicity and corrosion behavior of alkali-heat-treated magnesium in simulated body fluid. *Surf. Coat. Technol.* **185,** 92 (2004).
15. H. Kuwahara, Y. Al-Abdullat, N. Mazaki, S. Tsutsumi, and T. Aizawa: Precipitation of magnesium apatite on pure magnesium surface during immersing in Hank's solution. *Mater. Trans., JIM* **42,** 1317 (2001).
16. R. Rettig and S. Virtanen: Composition of corrosion layers on a magnesium rare-earth alloy in simulated body fluids. *J. Biomed. Mater. Res.* **88A,** 359 (2004).
17. Y.C. Xin, C.L. Liu, X.M. Zhang, G.Y. Tang, X.B. Tian, and P.K. Chu: Corrosion behavior of biomedical AZ91 magnesium alloy in simulated body fluids. *J. Mater. Res.* **22,** 2004 (2007).
18. S.B. Cho, K. Nakanishi, T. Kokubo, N. Soga, C. Ohtsuki, T. Nakamura, T. Kitsugi, and T. Yamauro: Dependence of apatite formation on silica-gel on its structure—Effect of heat-treatment. *J. Am. Ceram. Soc.* **78,** 1769 (1995).
19. G.L. Song and A. Atrens: Corrosion mechanisms of magnesium alloys. *Adv. Eng. Mater.* **1,** 11 (1999).
20. S.V. Golubev, O.S. Pokrovsky, and V.S. Savenko: Unseeded precipitation of calcium and magnesium phosphates from modified seawater solutions. *J. Cryst. Growth* **205,** 354 (1999).
21. W. Tongamp, Q.W. Zhang, and F. Saito: Preparation of meixnerite (Mg-Al-OH) type layered double hydroxide by a mechanochemical route. *J. Mater. Sci.* **42,** 9210 (2007).
22. J. Weng, Q. Liu, J.G.C. Wolke, X.D. Zhang, and K. deGroot: Formation and characteristics of the apatite layer on plasma-sprayed hydroxyapatite coatings in simulated body fluid. *Biomaterials* **18,** 1027 (1997).
23. J. Martin, P. Dan, and T. Dominique: Corrosion product formation during NaCl induced atmospheric corrosion of magnesium alloy AZ91D. *Corros. Sci.* **49,** 1540 (2007).
24. L.T. Canham, C.L. Reeves, A. Loni, M.R. Houlton, J.P. Newey, A.J. Simons, and T.I. Cox: Calcium phosphate nucleation on porous silicon: Factors influencing kinetics in acellular simulated body fluids. *Thin Solid Films* **297,** 304 (1997).
25. L.M. Epure, S. Dimitrievska, Y. Merhi, and L.H. Yahia: The effect of varying Al_2O_3 percentage in hydroxyapatite/Al_2O_3 composite materials: Morphological, Chemical and cytotoxic evaluation. *J. Biomed. Mater. Res.* **83,** 1009 (2007).
26. M.A. Aramendia, V. Borau, C. Jiménez, J.M. Marinas, F.J. Romcro, J.A. Navío, and J. Barrios: Modification of the activity of $Mg_3(PO_4)_2$ in the gas-phase conversion of cyclohexanol by addition of sodium carbonate. *J. Catal.* **157,** 97 (1995).
27. D.V. Kilpadi, G.N. Raikar, J. Liu, Y. Vohra, and J.C. Gregory: Effect of surface treatment on unalloyed titanium implants: Spectroscopic analyses. *J. Biomed. Mater. Res.* **40,** 646 (1998).
28. N.C. Hosking, M.A. Strom, P.H. Shipway, and C.D. Rudd: Corrosion resistance of zinc-magnesium coated steel. *Corros. Sci.* **49,** 3669 (2007).
29. H.Y. Hsiao and W.T. Tsai: Characterization of anodic films formed on AZ91 D magnesium alloy. *Surf. Coat. Technol.* **190,** 299 (2005).
30. Y. Tanimoto, Y. Shibata, Y. Kataoka, T. Miyazaki, and N. Nishiyama: Osteoblast-like cell proliferation on tape-cast and sintered tricalcium phosphate sheets. *Acta Biomater.* **4,** 397 (2008).
31. E. Landi, S. Sprio, M. Sandri, G. Celotti, and A. Tampieri: Development of Sr and CO_3 co-substituted hydroxyapatites for biomedical applications. *Acta Biomater.* **4,** 656 (2008).
32. S.R. Kim, J.H. Lee, Y.T. Kim, D.H. Riu, S.J. Jung, Y.J. Lee, S.C. Chung, and Y.H. Kim: Synthesis of Si, Mg substituted hydroxyapatites and their sintering behaviors. *Biomaterials* **24,** 1389 (2003).
33. K. Soto, K.M. Garza, and L.E. Murr: Cytotoxic effects of aggregated nanomaterials. *Acta Biomater.* **3,** 351 (2007).